Title
Half-scale transverse shaking table test of a geosynthetic reinforced soil bridge abutment

Permalink
https://escholarship.org/uc/item/7tk8849s

Journal
Geosynthetics International, 25(6)

ISSN
1072-6349

Authors
Zheng, Y
McCartney, JS
Shing, PB
et al.

Publication Date
2018-12-01

DOI
10.1680/jgein.18.00019

Peer reviewed

Transverse shaking table test of a half-scale geosynthetic reinforced soil bridge abutment

---

Yewei Zheng[1], John S. McCartney[2], P. Benson Shing[3] and Patrick J. Fox[4]

[1] Postdoctoral Research Scholar, Department of Structural Engineering, University of California, San Diego, La Jolla, CA, 92093-0085, USA; E-mail: y7zheng@ucsd.edu; ORCID Number: 0000-0001-9038-4113 (Corresponding Author)

[2] Associate Professor, Department of Structural Engineering, University of California, San Diego, La Jolla, CA, 92093-0085, USA; E-mail: mccartney@ucsd.edu; ORCID Number: 0000-0003-2109-0378

[3] Professor and Chair, Department of Structural Engineering, University of California, San Diego, La Jolla, CA, 92093-0085, USA; E-mail: pshing@ucsd.edu

[4] Shaw Professor and Head, Department of Civil and Environmental Engineering, Pennsylvania State University, University Park, PA 16802, USA; E-mail: pjfox@engr.psu.edu; ORCID Number: 0000-0001-7279-3490

ABSTRACT: This paper presents a shaking table study on the seismic response of a half-scale geosynthetic reinforced soil (GRS) bridge abutment with modular block facing, focusing on the response subjected to shaking in the direction transverse to the bridge beam. The model geometry, geosynthetic reinforcement stiffness, backfill soil modulus, bridge surcharge stress, and characteristics of the earthquake motions were scaled according to established similitude relationships for shaking table tests in a 1g gravitational field. The GRS bridge abutment was constructed using well-graded angular sand backfill and reinforced with uniaxial geogrid reinforcement layers in both the longitudinal and transverse directions. The facing displacements, bridge seat settlements, horizontal accelerations, vertical and lateral stresses, reinforcement strains, and bridge seat and bridge beam interactions were measured during a sequence of applied input motions. The average incremental residual bridge seat settlement is 4.7 mm after the Northridge motion, which corresponds to a vertical strain of 0.22% for the abutment. After a series of earthquake motions, the maximum residual strains occurred near the facing block connections for the lowermost layer, and under the bridge seat for higher layers.

KEYWORDS: Geosynthetics, Geosynthetic reinforced soil, Bridge abutment, Retaining wall, Shaking table test, Reduced-scale model

1. INTRODUCTION

Geosynthetic reinforced soil (GRS) bridge abutments are widely used in transportation infrastructure and provide many advantages over traditional pile-supported designs, including lower cost, faster and easier construction, and smoother transition between the bridge and approach roadway. However, use of this technology in high seismicity areas like California leads to questions regarding the expected ranges of dynamic and residual facing displacements, bridge seat settlements, and interactions between the bridge beam and GRS bridge abutment.

Several experimental and numerical studies have been conducted on the response of GRS bridge abutments for static loading conditions (Wu et al. 2001, 2006; Adams et al. 2011, 2014; Iwamoto et al. 2015; Nicks et al. 2013, 2016; Helwany et al. 2003, 2007; Fakharian and Attar 2007; Ambauen et al. 2016; Zheng and Fox 2016, 2017; Zheng et al. 2014, 2015, 2017a). However, fewer studies have investigated the response of GRS bridge abutments for seismic loading conditions. Helwany et al. (2012) investigated the dynamic response a 3.6 m-high GRS bridge abutment subjected to shaking in the longitudinal direction, and the abutment remained functional with some damage to the bottom corner blocks for horizontal base accelerations up to 1.0*g*. Zheng et al. (2017b, 2017c) performed shaking table tests on a 2.7 m-high half-scale GRS bridge abutment with shaking in the longitudinal direction, and observed relatively small deformations after earthquake motions with peak ground accelerations (PGA) of 0.31*g* and 0.40*g*. Although the observations from this limited number of studies indicate that GRS bridge abutments may have satisfactory seismic performance during longitudinal shaking, GRS bridge abutments in the field are subjected to three-dimensional (3D) shaking during earthquakes. Because the constraints for movement are different in the directions longitudinal and transverse to the bridge beam (i.e., the longitudinal and transverse directions), shaking in the transverse direction (i.e., transverse shaking) may lead to a different deformation response than that observed for shaking in the longitudinal direction (i.e., longitudinal shaking). Further, Zheng et al. (2017b) observed that longitudinal shaking will lead to deformations in the transverse direction that are of similar magnitude as those observed in the longitudinal direction. Therefore, additional shaking table tests would be helpful to evaluate the seismic performance of GRS bridge abutments for shaking in different directions.

This paper presents the results from shaking table tests on a half-scale GRS bridge abutment subjected to transverse shaking to understand the facing displacements, bridge seat settlements, acceleration response, vertical and lateral stresses, and bridge seat and bridge beam interactions. The results are compared with those from shaking table tests on a similar half-scale GRS bridge abutment subjected to longitudinal shaking, as reported by Zheng et al. (2017b) and Zheng (2017), to investigate the effect of shaking direction on 3D deformation response.

2. BACKGROUND

Although only a few shaking tests have been performed on GRS bridge abutments, shaking table tests have been widely used to investigate the dynamic response of GRS walls. Due to the limitation of size and payload capacity of typical shaking tables, many of these tests have been conducted on reduced-scale models, in which similitude relationships must be considered in the test design to produce a similar response between a reduced-scale model specimen and the full-scale prototype structure. The similitude relationships proposed by Iai (1989) have been widely used for 1g shaking table testing on reduced-scale reinforced soil structures (El-Emam and Bathurst 2004, 2005, 2007; Guler and Enunlu 2009; Sabermahani et al. 2009; Guler and Selek 2014; Latha and Santhanakumar 2015; Panah et al. 2015). Although reduced-scale model tests are less costly and easier to conduct, shaking table tests on full-scale GRS walls with the actual materials and construction techniques used in the field are preferred when possible (e.g., Ling et al. 2005, 2009, 2012; Fox et al. 2015).

El-Emam and Bathurst (2004, 2005, 2007) performed a series of shaking table tests on 1 m-high, 1/6th-scale GRS walls with a full-height rigid facing panel using a stepped-amplitude sinusoidal motion. Results indicated that facing displacements could be reduced by using a smaller facing panel mass, an inclined facing panel, longer reinforcement, stiffer reinforcement, and smaller vertical reinforcement spacing. Ling et al. (2005) reported a series of large-scale shaking table tests on 2.8 m-high GRS walls with modular block facing and sand backfill. Experimental results showed that the GRS walls experienced negligible deformations under a moderate earthquake motion (PGA = 0.40*g*) and performed well under a strong earthquake motion (PGA = 0.86*g*). Facing displacements were reduced by increasing reinforcement length for top layers and reducing reinforcement vertical spacing. The vertical component of the earthquake motion was found to have little effect on wall deformations and accelerations, but increased the reinforcement tensile forces. Fox et al. (2015) conducted a shaking table test on a 6.1 m-high full-scale GRS wall with modular block facing. The GRS wall experienced a permanent displacement of 56 mm at the top after a series of sinusoidal and earthquake motions. The ultimate state of the GRS wall indicated moderate damage but no collapse.

Helwany et al. (2012) reported shaking table tests on a 3.6 m-high GRS bridge abutment with modular block facing. The GRS bridge abutment had poorly-graded gravel backfill and was reinforced using a woven polypropylene geotextile with a vertical spacing of 0.2 m. The GRS bridge abutment was subjected to a series of horizontal sinusoidal motions in the longitudinal direction with increasing amplitude. No damage was observed until the horizontal base acceleration reached 0.67g, and no significant distress occurred for horizontal base accelerations up to 1.0g. The incremental bridge seat settlement was approximately 50 mm when the peak horizontal acceleration increased from 0.67g to 1.0g. Zheng et al. (2017b, 2017c) conducted shaking table tests on a half-scale GRS bridge abutment with modular block facing subjected to a series of earthquake motions in the longitudinal direction. The abutment model was reinforced with uniaxial geogrids in both the longitudinal and transverse directions at a vertical spacing of 0.15 m and had well-graded angular sand backfill. Results indicated that the GRS bridge abutment experienced small deformations for two earthquake motions with PGA of 0.31g and 0.40g, with model-scale maximum incremental residual facing displacements of 1.0 mm and average incremental residual bridge seat settlements of 1.4 mm.

3. EXPERIMENTAL PROGRAM

3.1. Similitude relationships

The shaking table tests were conducted using the indoor shaking table at the University of California, San Diego (UCSD) Powell Structural Laboratory, which was refurbished prior to this study to increase the fidelity of dynamic motion (Trautner et al. 2017). The shaking table has areal footprint dimensions of 5 m × 3 m and a maximum payload capacity of 356 kN. Considering the size and payload capacity of the table, a length scaling factor of $\lambda = 2$, defined as the ratio of prototype length to model length, was selected for the current study. The similitude relationships proposed by Iai (1989) were used for the half-scale shaking table tests. The model geometry, geosynthetic reinforcement stiffness, backfill soil modulus, bridge surcharge stress, and characteristics of the earthquake motions were scaled using the factors given in Table 1.

3.2. Materials

The backfill soil has coefficient of uniformity C_u = 6.1 and coefficient of curvature C_z = 1.0, and is classified as well-graded angular sand (SW) according to the Unified Soil Classification System (USCS). The mean particle size D_{50} = 0.85 mm and corresponds to a prototype value of 1.7 mm, which still falls within the sand-size range, and the corresponding prototype sand is also classified as SW. The specific gravity is 2.61, and the maximum and minimum void ratios are 0.853 and 0.371, respectively. The standard Proctor compaction curve for this sand is relatively flat, as reported by Zheng et al. (2017b), which indicates that the compaction water content does not have a significant effect on the dry unit weight for this sand. The target soil compaction conditions for construction of the GRS bridge abutment model were gravimetric water content w_c = 5% and relative density D_r = 70%, the latter of which was selected to meet the similitude relationships. A series of triaxial compression tests were conducted on dry sand specimens with different relative densities and yielded a secant modulus at 0.5% axial strain for D_r = 70% and effective confining stress σ' = 34 kPa that was approximately one-half that for D_r = 85% and σ' = 69 kPa. A relative density of 85% corresponds to a relative compaction of 96% according to the standard Proctor compaction effort, which is within the typical range of field compaction requirements for GRS bridge abutments (Berg et al. 2009, Adams et al. 2011). For D_r = 70%, the dry backfill sand has a peak tangent friction angle ϕ'_p = 51.3° and zero cohesion. The apparent cohesion associated with compacting the sand to different water contents can be accounted for using the suction stress concept of Lu et al. (2010), which employs parameters from triaxial tests on the dry sand and the soil-water retention curve (SWRC). The average dilation angle ψ = 13° according to volumetric strains ranging from the axial strain at the point of maximum contraction to an axial strain of 5%.

The geosynthetic reinforcement is a uniaxial high density polyethylene (HDPE) geogrid (Tensar LH800). As reported by Zheng (2017) from tensile tests on single rib specimens, the geogrid has secant stiffness at 5% strain $J_{5\%}$ = 380 kN/m and ultimate strength T_{ult} = 38 kN/m in the machine direction, and $J_{5\%}$ = 80 kN/m and T_{ult} = 4 kN/m in the cross-machine direction. Using the similitude relationships in Table 1, the corresponding tensile stiffness and ultimate strength in the machine direction for the prototype geogrid are 1520 kN/m and 152 kN/m, respectively, which are in the typical range for prototype structures in the field.

Concrete modular facing blocks with dimensions of 0.30 m × 0.25 m × 0.15 m were selected to meet the similitude relationships. A layer of geogrid reinforcement was placed between each course of blocks for over 80% of the block-to-block contact surface. Fiberglass pins were inserted through the geogrid apertures to assist with block alignment and are not expected to enhance the block-geogrid connection, which was essentially frictional.

3.3. Model configuration and construction

The shaking table test configuration of the bridge system is shown in Figure 1. The bridge beam is placed on a bridge seat resting on the GRS bridge abutment at one end and on a concrete support wall resting on a sliding platform at the other end. The concrete bridge beam has dimensions of 6.4 m (length) × 0.9 m (width) × 0.45 m (height) and a self-weight of 65 kN. Additional dead weights (steel plates) of 33 kN are evenly distributed and rigidly attached to the beam to produce a total weight of 98 kN, which produces an average vertical stress of 121 kPa on top of the bridge seat. The bridge seat has a self-weight of 7 kN and a bottom surface with plan dimensions of 0.65 m × 1.30 m. The average vertical contact stress on the backfill soil from the bridge seat bottom surface due to the total weight of bridge seat, bridge beam, and dead weights is 66 kPa, which corresponds to a prototype vertical stress of 132 kPa and is in the typical range for GRS bridge abutments in the field (Adams et al. 2011). On the other end, the bottom of the concrete support wall rests on a low friction sliding platform, based on a design concept from Fox et al. (1997, 2006), and is rigidly connected to the shaking table using steel connection beams to transmit motions from the shaking table. Braces were welded to the connection beams to increase stiffness in the transverse direction. Elastomeric bearing pads with a thickness of 25 mm and plan dimensions of 0.45 m × 0.90 m were placed under both ends of the bridge beam. The seismic joint (i.e., vertical gap) between the bridge beam and each side wall of the bridge seat is 25 mm wide. During shaking, the bridge beam interacts with the GRS bridge abutment and support wall through friction developed between the concrete and the bearing pads, and the bridge beam may potentially contact the sides of the bridge seat.

The GRS bridge abutment has modular block facing on three sides, including a front wall facing perpendicular to the length of the bridge beam and two side wall facings parallel to the length of the bridge beam. The back of the GRS bridge abutment is supported by a rigid reaction wall consisting of a steel frame with plywood face. The reaction wall was designed to be sufficiently stiff to provide at-rest conditions during construction and experience minimal deflections during shaking, which was verified by Zheng et al. (2017b). A top view diagram is shown in Figure 2(a) and cross-sectional view diagrams in the longitudinal and transverse directions are shown in Figures 2(b) and 2(c), respectively. The abutment has plan dimensions of 1.72 m × 2.10 m, including the wall facing blocks. The bridge seat rests on top of the lower GRS wall and has a setback distance of 0.15 m from each of the three wall facings. There is no backfill soil between the bridge seat and side wall facings in the transverse direction due to limited space, which results in no soil confinement on the two sides of the bridge seat. The GRS bridge abutment has a total height of 2.7 m, consisting of a 2.1 m-high lower GRS wall and a 0.6 m-high upper wall, resting on a 0.15 m-thick foundation soil layer placed directly on the shaking table. The clearance distance between the top of the front wall facing and bottom of the bridge beam is 0.15 m. The GRS bridge abutment specimen corresponds to a prototype structure with a total height of 5.4 m and a bridge clearance height of 4.5 m, the latter of which meets FHWA requirements (Stein and Neuman 2007).

The foundation soil layer was the same as the backfill soil and was first placed within a wooden frame bolted to the shaking table at a higher relative density (D_r = 85%) than the backfill sand to provide a firm base for the GRS bridge abutment. The lower GRS wall was constructed in fourteen 0.15 m-thick soil lifts. Each lift includes uniaxial geogrid reinforcement layers placed horizontally within the backfill soil in the longitudinal and transverse directions, with frictional connections between the facing blocks. The longitudinal reinforcement layers extended 1.47 m from the front wall facing into the backfill soil. The transverse reinforcement layers extended 0.8 m from each side wall facing to meet (without connection) at the center. The reinforcement configuration for this test is the same as for the reinforced soil zone in the longitudinal shaking test (Zheng et al. 2017b). The transverse reinforcement layers and side wall facing blocks are offset by 25 mm vertically from the longitudinal reinforcement layers and front wall facing blocks. This offset was needed to avoid direct contact between longitudinal and transverse geogrid layers and maintain interaction between the geogrid and backfill soil. Although not necessary in actual GRS bridge abutments, this offset technique was used for the current study due to geometric constraints of the shaking table.

Sand cone tests were used to measure the as-constructed dry unit weights of the backfill sand during construction, and corresponding values of relative density range from 65% to 76%, with an average of 71%. The measured gravimetric water contents of the different compacted soil lifts range from 3.4% to 6.7%, with an average of 5.0%. Considering that the compaction curve is relatively flat for this sand, the variation in gravimetric water content is unlikely to significantly affect the compacted dry unit weight. Apparent cohesion can have an important effect on the ultimate state of GRS walls (Vahedifard et al. 2014, 2015), and the shear modulus is expected to vary as well (Khosravi et al. 2010). Using the soil-water retention curve (SWRC) for this sand reported by Zheng et al. (2017b), the apparent cohesion estimated using the suction stress concept of Lu et al. (2010) was found to be relatively uniform with an average value of 2 kPa.

3.4. Instrumentation

Data was collected during shaking for 160 channels at a simultaneous sampling rate of 256 Hz. Sensors included string potentiometers, linear potentiometers, accelerometers, total pressure cells, load cells, and strain gauges. Sensor details are provided by Zheng et al. (2017b). Figure 3 shows the instrumentation for the transverse section T1, located at distance from the front wall facing x = 0.48 m, and for the longitudinal centerline section L1 located at distance from the north side wall facing y_n = 0.8 m. The T1 and L1 sections are indicated in Figure 2(a). Horizontal displacements for the side wall facing blocks at different elevations, bridge seat, bridge beam, and support wall in the transverse direction were measured using string potentiometers, and horizontal displacements of the front wall facing blocks were measured using linear potentiometers. String potentiometers were used to measure settlements at the four corners of the bridge seat (Figure 2a). String potentiometers were mounted on rigid reference frames apart from the shaking table and had sufficient tension to measure dynamic motions within the frequency band for the test. The string potentiometer measurements were corrected using measured horizontal displacements of the shaking table in the transverse direction to yield relative displacements with respect to the table. Accelerometers were attached to the wall facing blocks and placed within the backfill soil to measure horizontal accelerations in the transverse direction. Earth pressure cells were placed in the backfill soil to measure vertical and horizontal total stresses. Two load cells were embedded in the south and north sides of the west end of bridge beam, respectively, to measure potential contact forces between the bridge beam and bridge seat during shaking. Geogrid tensile strains were measured using strain gauges mounted in pairs at the mid-point of longitudinal ribs, with one gauge on top and the other on bottom to correct for rib bending (Bathurst et al. 2002). Considering that strain gauge measurements may be affected by attachment technique and non-uniform stiffness along a rib (Bathurst et al. 2002), tensile tests were conducted to obtain a correction factor (CF), defined as the ratio of global strain to gauge strain. The CF is 1.1 and is not significantly affected by loading rate (Zheng et al. 2017b). All measured geogrid strains were corrected using this CF value.

3.5. Input motions

A series of input motions, including white noise and earthquake motions, were applied to the GRS bridge abutment system in the transverse direction (i.e., north-south direction in Figure 2) in sequence, with a minimal pause (approximately 5 minutes) between each motion. The shaking table was operated in acceleration-control mode for the white noise motions and displacement-control mode for the earthquake motions. A summary of the first seven input motions, alternating between white noise and earthquake motions, is presented in Table 2. This paper focuses on the results for the three earthquake motions, and the results for the white noise motions can be found in McCartney et al. (2018).

Shaking table tests were conducted using motions scaled from the strike-slip 1940 Imperial Valley earthquake (El Centro station), the subduction zone 2010 Maule earthquake (Concepcion station), and the strike-slip 1994 Northridge earthquake (Newhall station) records. Examples of the acceleration and displacement time histories for the original and scaled Northridge motions are shown in Figure 4. The original motion has a peak ground acceleration (PGA) of 0.58g and peak ground displacement (PGD) of 177.4 mm. The scaled acceleration motion was obtained by maintaining the acceleration amplitudes and scaling (increasing) the frequencies by a factor of $\sqrt{2}$ as indicated in Table 1. The scaled displacement time history was obtained by double integration of the scaled acceleration, and has a PGD of 88.7 mm, which is one-half of the PGD for the original record. Scaled motions for the Imperial Valley and Maule earthquake records were obtained similarly and yield PGD values of 65.2 mm and 108.0 mm, respectively.

4. RESULTS

Test results are presented for testing system performance, facing displacements, bridge seat settlements, accelerations, reinforcement strains, and bridge seat and bridge beam interactions during the application of a series of earthquake motions in the transverse direction. Horizontal displacements and accelerations toward the north (see Figure 2), outward displacements for the front wall and side wall facings, and downward displacements (settlements) for the bridge seat are defined as positive, and elevation z is measured upward from the foundation soil. All presented results correspond to model-scale and should be adjusted using the similitude relationships (Table 1) to obtain corresponding values for the prototype structure. This study also includes comparisons with results reported by Zheng et al. (2017b) from shaking table tests on a similar GRS bridge abutment subjected to longitudinal shaking. It should be noted that the GRS bridge abutment subjected to transverse shaking in the current study include no retained soil zone behind the reinforced soil zone due to the geometric constraints of the table, whereas the GRS bridge abutment for the longitudinal shaking test had a 0.63 m-long retained soil zone (Zheng et al. 2017b).

4.1. Testing system performance

In addition to the GRS bridge abutment on the shaking table, the table was also used to drive the support wall at the opposite end of the bridge beam. Characterization of the testing system performance (i.e., shaking table and connected support wall resting on the sliding platform) is important for the transverse shaking test because the configuration of a support wall connected to one side of the shaking table is a unique design and has not been used in previous shaking table experiments. The performance of the testing system was evaluated based on the measured displacement and acceleration response in the direction of shaking. A summary of the target and measured peak response of the shaking table for the three earthquake motions is presented in Table 2. The actual peak displacements for the shaking table are essentially the same as the target values, whereas the actual peak accelerations are larger than the target values.

The measured testing system response for the Northridge motion is shown in Figure 5. In Figure 5(a), the measured displacement time history of the shaking table is in close agreement with the target (i.e., specified) displacements, whereas the support wall was also in good agreement but displays larger peak displacements due to the inertial forces of the support wall and some noise, which may be attributed to resonance of the support wall during shaking. In Figure 5(b), the measured acceleration time history of the shaking table generally matches well with the target accelerations, but shows larger peak values. The measured PGA of 0.86*g* for the shaking table is larger than the target value of 0.58*g*. This is likely due to the inertia of the table itself and friction developed on the table bearings associated with the heavy payload. A comparison of the response spectra (5% damping) of the shaking table, support wall, and target motions is shown in Figure 5(c). The pseudo-spectral accelerations of the shaking table and target motions are in good agreement for frequencies less than 10 Hz, which indicates that the shaking table adequately reproduced the salient characteristics of the target motion. The pseudo-spectral accelerations for the support wall are different from the target values because the fundamental frequency of 3.6 Hz for the support wall is in the frequency range for typical earthquake motions. The support wall was out of phase with the table motion during shaking due to the flexibility of the connection beam frame. Considering that the support wall interacted with the GRS bridge abutment indirectly through the bridge beam, the out of phase behavior of the support wall likely did not significantly affect the behavior of GRS bridge abutment.

4.2. Facing displacements

Time histories of incremental facing displacements for the modular block walls at the south and north sides of the transverse section T1 (i.e., T1-South and T1-North, as shown in Figure 3), during the Northridge motion are shown in Figure 6. Values of incremental facing displacement are taken relative to the initial facing displacements before the shaking event. Results show that the two side walls moved in-phase during shaking; thus, one facing moved outward as the other facing moved inward. Figure 6 also indicates that each wall experienced larger facing displacements at higher elevations and permanent (i.e., residual) deformations by the end of the test. Facing displacement profiles corresponding to the specific times of maximum dynamic facing displacements for the T1-South and T1-North walls during the Northridge motion are shown in Figure 7. At t = 3.00 s, the T1-North wall reached the maximum outward (i.e., positive) displacement, whereas the T1-South wall had inward (i.e., negative) displacement of similar magnitude. At t = 4.09 s, the T1-South wall reached its maximum outward displacement and shows a similar profile shape. The behavior of the transverse section under seismic loading is similar to soil behavior when subjected to simple shear conditions.

Incremental maximum dynamic and residual facing displacement profiles for the three walls and three earthquake motions are shown in Figure 8, and the maximum value from each profile is provided in Table 3. The earthquake motions produced generally similar responses from the GRS bridge abutment model, although some differences are noted. Maximum facing displacements were measured near or at the highest elevation (z = 1.875 m) for each wall and increased with increasing motion PGA. For the Imperial Valley motion, maximum dynamic displacement profiles for the side walls (i.e., T1-South and T1-North) are in close agreement and indicate peak values of approximately 5 mm. For the Maule test, the side walls display dissimilar maximum displacements of 17.0 mm for T1-South and 9.3 mm for T1-North. The dissimilar response was more pronounced for side walls in the Northridge motion, with a maximum displacement for the T1-North wall (34.7 mm) more than double that for the T1-South wall (13.3 mm). Differences in deformation behavior for the side walls are attributed to asymmetry of the earthquake motions and are more significant with increasing motion PGA. The front wall facing for longitudinal section L1 experienced much lower displacements because shaking was parallel to the plane of the wall. Maximum dynamic displacements for this wall were 1.6 mm, 3.2 mm, and 4.0 mm for the Imperial Valley, Maule, and Northridge motions, respectively. These values indicate that shaking in the transverse direction also produced facing displacements in the longitudinal direction and thus illustrate the multi-directional deformation response of the GRS bridge abutment model for uni-directional shaking conditions.

After shaking was completed, facing displacements were largely recovered for the side walls, especially at higher elevations. The maximum residual facing displacements were in close agreement (approximately 1 mm) for the Imperial Valley motion and ranged from 0 to 2 mm for the Maule motion and from -5 mm to 10 mm for the Northridge motion. These residual values also indicate progressively asymmetric deformation behavior of the side walls with increasing motion PGA. The maximum residual facing displacement for L1 was 3.2 mm (Northridge motion). Residual facing displacements are all less than 10 mm, and mostly less than 5 mm, which would be multiplied by a factor of $\lambda = 2$ for the prototype structure.

4.3. Bridge seat settlements

Settlements were measured at the four corners of the bridge seat during static and dynamic loading using string potentiometers, as shown in Figure 2(a). One of the string potentiometers on the northwest (NW) corner did not function during placement of the bridge beam and was replaced before the shaking tests. Settlement time histories at the bridge seat corners, along with average values, are shown during placement of the bridge beam in Figure 9(a). These settlements did not occur uniformly and a sudden but small shift was observed after 3 hours. The explanation for this shift is unknown. After 5 hours, the settlements stabilized and indicate negligible creep. Also, a slight tilting of the bridge seat toward the south side occurred due to placement of the bridge beam. The average settlement on the south side of the bridge seat (SW and SE) was 2.1 mm and the average settlement on the north side (NE) was 1.0 mm. After 94 hours, the average bridge seat settlement was 1.6 mm, which corresponds to a vertical strain of 0.08% for the 2.1 m-high lower GRS wall.

Time histories of incremental bridge seat settlement for the four corners during the Northridge motion are shown in Figure 9(b). At t = 4.13 s, the south side of the bridge seat (SW and SE) had a dynamic settlement of 6.7 mm, whereas the north side (NW and NE) had a negative settlement (i.e., uplift) of 4.1 mm, which indicates rocking of the bridge seat in the N-S direction (i.e., the direction of shaking). The residual settlement on the south side (SW and SE) is larger than on the north side (NW and NE), which indicates that the bridge seat tilted further toward the south after shaking. The average settlement time history of the bridge seat is shown in Figure 10 (transverse shaking) and indicates an average maximum dynamic settlement of 6.1 mm and an average minimum dynamic value of -2.1 mm. The average residual settlement of the bridge seat is 4.7 mm, which corresponds to a vertical strain of 0.22%. As shown in Table 4, the maximum dynamic settlement is 3.3 mm for the Imperial Valley motion and 9.5 mm for the Maule motion. The residual bridge seat settlements are 2.5 mm and 4.8 mm for the Imperial Valley and Maule motions, respectively, and yield vertical strains of 0.12% and 0.23%.

Zheng et al. (2017b) reported shaking table test results for a similar GRS bridge abutment subjected to the same earthquake motions in the longitudinal direction. Average incremental bridge seat settlements from this test are also shown in Figure 10 for comparison. Table 5 presents the average incremental residual bridge seat settlements for longitudinal and transverse shaking with the three earthquake motions. For the Northridge motion, the maximum dynamic settlement for transverse shaking is 6.1 mm, which is smaller than the value of 7.0 mm for longitudinal shaking. However, the residual settlement of 4.7 mm for transverse shaking is greater than the value of 2.2 mm for longitudinal shaking. Similarly, for the Imperial Valley and Maule motions, the residual bridge seat settlements for transverse shaking are larger than for longitudinal shaking. The larger settlements for the transverse shaking test are attributed to the lack of lateral confinement for the side walls and resulting simple shear deformation response of the abutment, whereas the reaction wall provided confinement on the back of the abutment for the longitudinal shaking test. Another likely contributing factor was the lack of soil confinement on the two sides of the bridge seat in the transverse direction, whereas the backwall of the bridge seat was confined by backfill soil in the longitudinal direction.

4.4. Accelerations

Horizontal accelerations were measured at selected elevations on the side wall facings and within the backfill soil for transverse section T1 (Figure 3a). The root-mean-square (RMS) method was used to mitigate effects of high frequency noise and also characterize amplitude and frequency content in the measured response (Kramer 1996; El-Emam and Bathurst 2005). RMS acceleration ratio profiles for the facing blocks and reinforced soil zones for the T1-South and T1-North walls, normalized by the actual RMS acceleration of the shaking table to yield amplification ratios, are shown in Figure 11. The acceleration profiles show consistent trends for the three earthquake motions and are in close agreement for the two side walls. Accelerations for each side wall increase nonlinearly with increasing elevation for the facing block and the reinforced soil zone, with slightly higher values for the facing blocks likely due to inertial forces associated with the facing blocks. Interestingly, the data indicate that amplification ratios are highest for the Imperial Valley motion, up to 1.4, and decrease with increasing motion PGA. The difference in acceleration amplification ratios for the three earthquake motions may be attributed to characteristics of the earthquake motions relative to the stiffness of the GRS bridge abutment, such as PGA and frequency content, and may be influenced by different initial conditions of the abutment before each shaking test due to progressive softening of the structure associated with sequential application of the earthquake motions. Further investigations are needed using a validated numerical model to understand the changes in acceleration amplification ratios for the sequence of earthquake motions.

4.5. Vertical and lateral stresses

Vertical and lateral stresses were measured behind the T1-South and T1-North side wall facings at the locations shown in Figure 3(a). Profiles for the initial (before shaking), maximum dynamic (during shaking), and residual (after shaking) vertical stresses during the Northridge motion are shown in Figure 12(a). The initial vertical stresses for T1-South were larger than those for T1-North, which may reflect tilting of bridge seat toward the south side as observed in the bridge seat settlement data (Figure 9a). During shaking, the maximum vertical stresses are 130.9 kPa and 107.0 kPa for T1-South and T1-North, respectively, and both occurred at the mid-height of the wall. After shaking, the residual vertical stresses at the bottom are slightly larger than the initial values, which may reflect changes of soil arching in the backfill soil due to strong shaking.

Corresponding lateral stress profiles for the Northridge motion are shown in Figure 12(b). The initial lateral stresses for T1-South and T1-North are different, likely due to sequential application of the earthquake motions. The magnitudes of lateral stress are generally small (less than 8 kPa). During shaking, the maximum dynamic lateral stress is 18.2 kPa at the bottom of the wall for T1-South and is 13.6 kPa at the top for T1-North. The residual lateral stresses are generally close to the initial values for both sections.

4.6. Reinforcement strains

Distributions of residual reinforcement tensile strain for the T1-South and T1-North walls are shown in Figure 13. At the end of construction (EOC), tensile strains for both walls show similar magnitudes for reinforcement layers 1, 4, and 7, and different magnitudes for layers 10 and 13. Tensile strains in layers 10 and 13 under the bridge seat for T1-South are larger than those for T1-North, which again is attributed to the tilting of the bridge seat toward the south side during placement of the bridge beam (Figure 9a). In general, at the end of construction, the maximum tensile strains occurred near the facing block connections in layers 1 and 4, and at distance of 0.33 m from each side wall facing in layers 7, 10, and 13. After each earthquake motion, residual strains under the bridge seat increased significantly due to shaking. For instance, the residual strain at y_s = 0.33 m in layer 10 for T1-South was 0.13% at the end of construction, 0.23% after the Imperial Valley motion, 0.30% after the Maule motion, and 0.36% after the Northridge motion. Residual strains near the facing block connections increased for the lowermost layers and not for higher layers. In general, the maximum residual strains occurred near the facing block connections for the lowermost layer, and under the bridge seat for higher layers after shaking.

Reinforcement strain distributions for the T1-South and T1-North walls with initial (before shaking), maximum (during shaking), minimum (during shaking), and residual (after shaking) values during the Northridge motion are shown in Figure 14. The tensile strains near the facing block connections experienced significant increases during shaking. For instance, the tensile strain near the facing block connection in layer 7 for T1-South increased from an initial value of 0.04% to a maximum dynamic value of 0.51%. However, residual strains near the facing block connections for all layers are nearly equal to the initial values, which indicates that most of the dynamic reinforcement strains are recovered after shaking is completed. Nonetheless, the magnitudes of the maximum dynamic reinforcement strains near the facing block connections indicate that consideration of reinforcement connection strengths in the transverse direction is as important as for the longitudinal direction in seismic design.

Corresponding reinforcement strain distributions for the L1 front wall during the Northridge motion are shown in Figure 15. In general, tensile strains for the lowermost layer experienced little change during shaking, whereas greater changes occurred for higher layers. The magnitudes of reinforcement strain for the front wall are smaller than for the side walls due to the direction of shaking. Regardless, the data indicate that shaking in the transverse direction caused increased strains in the reinforcement layers in the longitudinal direction, which is consistent with the observed trends for front wall facing displacements shown in Figure 8.

4.7. Bridge seat and bridge beam interactions

Time histories of incremental horizontal displacement for the bridge seat and bridge beam during the Northridge motion are shown in Figure 16(a). Positive values indicate movement toward the north from the EOC condition. The initial horizontal displacements for the bridge seat and bridge beam before the Northridge motion (i.e., due to Imperial Valley and Maule motions) are -1.3 mm and 17.3 mm, respectively. During the Northridge motion, the bridge seat and bridge beam show similar displacement trends. However, the bridge beam experienced larger horizontal displacements than the bridge seat, which indicates sliding of the bridge beam relative to the bridge seat on the concrete-bearing pad interface. The residual horizontal displacements for the bridge seat and bridge beam are -18.8 mm and -10.8 mm, respectively. The time history of horizontal displacement for the bridge beam relative to the bridge seat during the Northridge motion is shown in Figure 16(b). During shaking, the bridge beam experienced a maximum relative displacement of 20.2 mm toward the south and 4.4 mm toward the north, and had a residual relative displacement of 10.6 mm toward the south after shaking.

As the bridge beam moved relative to the bridge seat, the width of the seismic joints varied during shaking. Horizontal contact forces between the bridge seat and bridge beam occur when the width of seismic joint reduces to zero. The time history of joint width on the north side during the Northridge motion also is shown in Figure 16(b). The initial joint width on the north and south sides before the Northridge motion was 4.4 mm and 45.6 mm, respectively. During shaking, joint closure occurred once on the north side at t = 3.02 s, resulting in a horizontal contact force of 17.9 kN, as shown in Figure 17. This corresponds to a contact force of 143.2 kN for the prototype structure, which is relatively small and would not be expected to cause damage to the concrete bridge seat. The joint reached a maximum width of 24.7 mm at t = 4.17 s. After the Northridge motion, the north joint remained open with a width of 15.1 mm, and the width of the south joint was 34.9 mm.

5. SUMMARY AND CONCLUSIONS

This paper presents a shaking table study of the seismic response of a half-scale GRS bridge abutment with modular block facing. The GRS bridge abutment was constructed using well-graded angular sand backfill and uniaxial geogrid reinforcement in both the longitudinal and transverse directions. A series of three scaled earthquake motions were applied to the GRS bridge abutment system in the transverse direction. The following conclusions are reached:

1. The two side walls for the transverse section of the abutment moved in-phase during shaking, which is similar to soil behavior when subjected to simple shear conditions. Incremental residual facing displacements after each scaled earthquake motion are less than 10 mm for the side walls. Shaking in the transverse direction also produced facing displacements for the front wall in the longitudinal direction with magnitudes less than 4 mm, which illustrates the multi-directional deformation response of the GRS bridge abutment model for uni-directional shaking conditions.
2. The average incremental residual bridge seat settlement is 4.7 mm for the Northridge motion, which corresponds to a vertical strain of 0.22% for the 2.1 m-high lower GRS wall. The average residual bridge seat settlements are 2.5 mm and 4.8 mm for the Imperial Valley and Maule motions, respectively, corresponding to vertical strains of 0.12% and 0.23%. Shaking in the transverse direction caused larger residual bridge seat settlements than shaking in the longitudinal direction for the conditions investigated.
3. Acceleration amplification ratio profiles for the facing block and reinforced soil zone are similar for the T1-South and T1-North side walls. Acceleration amplification ratios in the reinforced soil zone for the transverse section increase significantly with elevation for the Imperial Valley and Maule motions, and increase only slightly with elevation for the Northridge motion. The highest amplification ratio was 1.4, measured at the top of the T1-South wall facing for the Imperial Valley motion.
4. During the Northridge motion, the maximum dynamic vertical stresses were 130.9 kPa and

107.0 kPa for the T1-South and T1-North walls, respectively, and both occurred at the mid-height of the wall. Maximum dynamic lateral stresses were 18.2 kPa at the bottom of the T1-South wall and 13.6 kPa at the top of the T1-North wall.

5. After the series of earthquake motions was completed, the maximum residual tensile strains in the reinforcement occurred near the facing block connections for the lowermost layer, and under the bridge seat for higher layers. Reinforcement strains near the facing block connections for the side walls experienced a significant increase during shaking, which highlights the importance of considering reinforcement connection strength for the transverse direction in seismic design.
6. The bridge beam experienced permanent sliding relative to the bridge seat on the concrete-bearing pad during the Northridge motion. The vertical seismic joint closed at one point, producing a horizontal contact force of 17.9 kN between the bridge beam and bridge seat. This corresponds to a contact force of 143.2 kN for the prototype structure, which is relatively small and would not be expected to cause damage to the concrete bridge seat

Due to the limited size of the shaking table, the width of the GRS bridge abutment model in this study was smaller than a full-scale prototype GRS bridge abutment in the field, which likely led to a different 3D seismic response for the model than for the prototype. In particular, overlap of geogrid reinforcements in the transverse and longitudinal directions across the entire GRS bridge abutment may have produced an overly stiff response for the model, where such an overlap would be limited to the regions near the corners for the prototype. Also, the small bridge seat width may have permitted more rocking and experienced greater settlements than would be expected in a prototype GRS bridge abutment. Nonetheless, the results of this study provide valuable insights into the 3D seismic behavior of GRS bridge abutments subjected to transverse shaking and the experimental data that can be used for calibration of numerical models.

ACKNOWLEDGEMENTS

Financial support for this study provided by California Department of Transportation (Caltrans) Project 65A0556 with Federal Highway Administration (FHWA) Pooled Fund Members is gratefully acknowledged. The first author appreciates the GSI Fellowship provided by the Geosynthetic Institute. The authors thank Dr. Charles Sikorsky and Kathryn Griswell of Caltrans for their support and assistance with the project. The authors also thank the staff and undergraduate research assistants at the UCSD Powell Structural Laboratories for their help with the experimental work. The geogrids used in this study were provided by Tensar International Corporation.

NOTATIONS

Basic SI units are given in parentheses.

C_u coefficient of uniformity

C_z coefficient of curvature

D_{50} mean particle size (mm)

D_r relative density (%)

$J_{5\%}$ secant stiffness at 5% strain for geogrid (kN/m)

t time (s)

T_{ult} ultimate strength for geogrid (kN/m)

w_c gravimetric water content (%)

x distance from front wall facing (m)

y_n distance from north side wall facing (m)

y_s distance from south side wall facing (m)

z elevation above top of foundation soil (m)

λ scaling factor

σ' effective confining stress (kPa)

ϕ'_p peak friction angle (°)

REFERENCES

Adams, M., Nicks, J., Stabile, T., Wu, J., Schlatter, W. & Hartmann, J. (2011). Geosynthetic reinforced soil integrated bridge system interim implementation guide. *FHWA-HRT-11-026*, U.S. DOT, Washington, D.C.

Adams, M. T., Ooi, P. S. & Nicks, J. E. (2014). Mini-pier testing to estimate performance of full-scale geosynthetic reinforced soil bridge abutments. *Geotechnical Testing Journal*, Vol. 37, No. 5, 884-894.

Ambauen, S., Leshchinsky, B., Xie, Y. & Rayamajhi, D. (2016). Service-state behavior of reinforced soil walls supporting spread footings: a parametric study using finite-element analysis. *Geosynthetics International*, Vol. 23, No. 3, 156-170.

Bathurst, R. J., Allen, T. M. & Walters, D. L. (2002). Short-term strain and deformation behavior of geosynthetic walls at working stress conditions. *Geosynthetics International*, Vol. 9, Nos. 5-6, 451-482.

Berg, R. R., Christopher, B. R. & Samtani, N. (2009). Design and construction of mechanically stabilized earth walls and reinforced soil slopes – Volume I. *FHWA-NHI-10-024*, U.S. DOT, Washington, D.C.

El-Emam, M. M. & Bathurst, R. J. (2004). Experimental design, instrumentation and interpretation of reinforced soil wall response using a shaking table. *International Journal of Physical Modelling in Geotechnics*, Vol. 4, No. 4, 13-32.

El-Emam, M. M. & Bathurst, R. J. (2005). "Facing contribution to seismic response of reduced-scale reinforced soil walls. *Geosynthetics International*, Vol. 12, No. 5, 215-238.

El-Emam, M. M. & Bathurst, R. J. (2007). "Influence of reinforcement parameters on the seismic response of reduced-scale reinforced soil retaining walls. *Geotextiles and Geomembranes*, Vol. 25, No. 1, 33-49.

Fakharian, K. & Attar, I. H. (2007). Static and seismic numerical modeling of geosynthetic-reinforced soil segmental bridge abutments. *Geosynthetics International*, Vol. 14, No. 4, 228-243.

Fox, P. J., Andrew, A. C., Elgamal, A., Greco, P., Isaacs, D., Stone, M. & Wong, S. (2015). Large soil confinement box for seismic performance testing of geo-structures. *Geotechnical Testing Journal*, Vol. 38, No. 1, 72-84.

Fox, P. J., Rowland, M. G., Scheithe, J. R., Davis, K. L., Supple, M. R. & Crow, C. C. (1997). Design and evaluation of a large direct shear machine for geosynthetic clay liners. *Geotechnical Testing Journal*, Vol. 20, No. 3, 279-288.

Fox, P. J., Nye, C. J., Morrison, T. C., Hunter, J. G. & Olsta, J. T. (2006). Large dynamic direct shear machine for geosynthetic clay liners. *Geotechnical Testing Journal*, Vol. 29, No. 5, 392-400.

Guler, E. & Enunlu, A. K. (2009). Investigation of dynamic behavior of geosynthetic reinforced soil retaining structures under earthquake loads. *Bulletin of Earthquake Engineering*, Vol. 7, No. 3, 737-777.

Guler, E. & Selek, O. (2014). Reduced-scale shaking table tests on geosynthetic-reinforced soil walls with modular facing. *Journal of Geotechnical and Geoenvironmental Engineering*, 10.1061/(ASCE)GT.1943-5606.0001102, 04014015.

Helwany, S. M. B., Wu, J. T. H. & Froessl, B. (2003). GRS bridge abutments – an effective means to alleviate bridge approach settlement. *Geotextiles and Geomembranes*, Vol. 21, 177-196.

Helwany, S. M. B., Wu, J. T. H. & Kitsabunnarat, A. (2007). Simulating the behavior of GRS bridge abutments. *Journal of Geotechnical and Geoenvironmental Engineering*, Vol. 133, No. 10, 1229-1240.

Helwany, S. M. B., Wu, J. T. H. & Meinholz, P. (2012). Seismic design of geosynthetic-reinforced soil bridge abutments with modular block facing. *NCHRP Web-Only Document 187*, Transportation Research Board, Washington, D.C.

Iai, S. (1989). Similitude for shaking table tests on soil-structure-fluid models in 1g gravitational fields. *Soils and Foundations*, Vol. 29, No. 1, 105-118.

Iwamoto, M. K., Ooi, P. S., Adams, M. T. & Nicks, J. E. (2015). Composite properties from instrumented load tests on mini-piers reinforced with geotextiles. *Geotechnical Testing Journal*, Vol. 38, No. 4, 397-408.

Khosravi, A., Ghayoomi, M., McCartney, J. S. & Ko, H.-Y. (2010). “Impact of Effective Stress on the Dynamic Shear Modulus of Unsaturated Sands,” *GeoFlorida 2010: Advances in Analysis, Modeling & Design*, Orlando, FL, 410-419.

Kramer, S. L. (1996). *Geotechnical Earthquake Engineering*, Prentice Hall, Upper Saddle River, NJ, 653pp.

Latha, G. M. & Santhanakumar, P. (2015). Seismic response of reduced-scale modular block and rigid faced reinforced walls through shaking table tests. *Geotextiles and Geomembranes*, Vol. 43, No. 4, 307-316.

Ling, H. I., Leshchinsky, D., Wang, J., Mohri, Y. & Rosen, A. (2009). Seismic response of geocell retaining walls: experimental studies. *Journal of Geotechnical and Geoenvironmental Engineering*, Vol. 135, No. 4, 515-524.

Ling, H. I., Leshchinsky, D., Mohri, Y. & Wang, J. (2012). Earthquake response of reinforced segmental retaining walls backfilled with substantial percentage of fines. *Journal of Geotechnical and Geoenvironmental Engineering,* Vol. 138, No. 8, 934-944.

Ling, H. I., Mohri, Y., Leshchinsky, D., Burke, C., Matsushima, K. & Liu, H. (2005). Large-scale shaking table tests on modular block reinforced soil retaining walls. *Journal of Geotechnical and Geoenvironmental Engineering*, Vol. 131, No. 4, 465-476.

Lu, N., Godt, J. W. & Wu, D. T. (2010). "A Closed-form Equation for Effective Stress in Unsaturated Soil," *Water Resources Research*, Vol. 46, W05515, 10.1029/2009WR008646.

McCartney, J. S., Shing, P. B., Zheng, Y. & Rong, W. (2018). Interaction of MSE abutments with bridge superstructures under seismic loading – Phase II: Shaking table tests, California Department of Transportation (Caltrans), Sacramento, CA, USA.

Nicks, J. E., Adams, M. T., Ooi, P. S. K. & Stabile, T. (2013). Geosynthetic reinforced soil performance testing – axial load deformation relationships. *FHWA-HRT-13-066*, U.S. DOT, Washington, D.C.

Nicks, J. E., Esmaili, D. & Adams, M. T. (2016). Deformations of geosynthetic reinforced soil under bridge service loads. *Geotextiles and Geomembranes*, Vol. 44, No. 4, 641-653.

Panah, A. K., Yazdi, M. & Ghalandarzadeh, A. (2015). Shaking table tests on soil retaining walls reinforced by polymeric strips. *Geotextiles and Geomembranes*, Vol. 43, No. 2, 148-161.

Sabermahani, M., Ghalandarzadeh, A. & Fakher, A. (2009). Experimental study on seismic deformation modes of reinforced-soil walls. *Geotextiles and Geomembranes*, Vol. 27, No. 2, 121-136.

Stein, W. J. & Neuman, T. R. (2007). Mitigation strategies for design exceptions. *FHWA-SA-07-011*, U.S. DOT, Washington, D.C.

Trautner, C. A., Zheng, Y., McCartney, J. S. & Hutchinson, T. C. (2017). An approach for shake table performance evaluation during repair and retrofit actions. *Earthquake Engineering and Structural Dynamics*, 10.1002/eqe.2942.

Vahedifard, F., Leshchinsky, B., Sehat, S. & Leshchinsky, D., 2014, "Impact of Cohesion on Seismic Design of Geosynthetic-Reinforced Earth Structures," *Journal of Geotechnical and Geoenvironmental Engineering*, 10.1061/(ASCE)GT.1943-5606.0001099, 04014016.

Vahedifard, F., Leshchinsky, B., Mortezaei, K. & Lu, N., 2015, "Active Earth Pressures for Unsaturated Retaining Structures," *Journal of Geotechnical and Geoenvironmental Engineering*, 10.1061/(ASCE)GT.1943-5606.0001356, 04015048.

Wu, J. T. H., Ketchart, K. & Adams, M. (2001). GRS bridge piers and abutments. *Report No. FHWA-RD-00-038*, U.S. DOT, Washington, D.C.

Wu, J. T. H., Lee, K. Z. Z & Pham, T. (2006). Allowable bearing pressures of bridge sills on GRS abutments with flexible facing. *Journal of Geotechnical and Geoenvironmental Engineering*, Vol. 132, No. 7, 830-841.

Zheng, Y. (2017). Numerical simulations and shaking table tests of geosynthetic reinforced soil bridge abutments. *Ph.D. Dissertation*, University of California, San Diego, La Jolla, CA.

Zheng, Y. & Fox, P. J. (2016). "Numerical investigation of geosynthetic-reinforced soil bridge abutments under static loading. *Journal of Geotechnical and Geoenvironmental Engineering*, 10.1061/(ASCE)GT.1943-5606.0001452, 04016004.

Zheng, Y. & Fox, P. J. (2017). "Numerical investigation of the geosynthetic reinforced soil-integrated bridge system under static loading. *Journal of Geotechnical and Geoenvironmental Engineering*, 10.1061/(ASCE)GT.1943-5606.0001665, 04017008.

Zheng, Y., Fox, P. J. & McCartney, J. S. (2017a). "Numerical study of compaction effect on the static behavior of geosynthetic reinforced soil-integrated bridge system." *Geotechnical Frontiers 2017*, Orlando, FL, USA, 33-43.

Zheng, Y., Fox, P. J. & Shing, P. B. (2014). "Numerical simulations for response of MSE wall-supported bridge abutment to vertical load." *GeoShanghai 2014, International Conference on Geotechnical Engineering 2014*, ASCE, Reston, VA, USA, 493-502.

Zheng, Y., Fox, P. J. & Shing, P. B. (2015). "Numerical study of deformation behavior for a geosynthetic-reinforced soil bridge abutment under static loading." *IFCEE 2015, International Foundations Congress & Equipment Exposition 2015*, ASCE, Reston, VA, USA, 1503-1512.

Zheng, Y., Sander, A. C., Rong, W., Fox, P. J., Shing, P. B. & McCartney, J. S. (2017b). Shaking table test of a half-scale geosynthetic-reinforced soil bridge abutment. *Geotechnical Testing Journal*, 10.1520/GTJ20160268.

Zheng, Y., Sander, A. C., Rong, W., McCartney, J. S., Fox, P. J. & Shing, P. B. (2017c). Experimental design for half-scale shaking table test of a geosynthetic-reinforced soil bridge abutment. *Geotechnical Frontiers 2017*, Orlando, FL, 54-63.

Table 1. Similitude relationships for 1*g* shaking table tests (Iai 1989).

Variable	Scaling factor	Value of scaling factor
Length	λ	2
Material density	1	1
Strain	1	1
Mass	λ^3	8
Acceleration	1	1
Velocity	$\lambda^{1/2}$	1.414
Stress	λ	2
Modulus	λ	2
Stiffness	λ^2	4
Force	λ^3	8
Time	$\lambda^{1/2}$	1.414
Frequency	$\lambda^{-1/2}$	0.707

Table 2. Input motion data for the shaking table test program.

Shaking event	Input motion	Model-scale duration (s)	Target PGA (*g*)	Actual PGA (*g*)	Target PGD (mm)	Actual PGD (mm)
1	White noise	120.0	0.10	0.16	2.7	7.9
2	Imperial Valley	28.3	0.31	0.42	65.2	65.2
3	White noise	120.0	0.10	0.17	2.7	7.7
4	Maule	100.4	0.40	0.56	108.0	107.9
5	White noise	120.0	0.10	0.15	2.7	7.7
6	Northridge	28.3	0.58	0.86	88.7	88.6
7	White noise	120.0	0.10	0.15	2.7	8.1

Table 3. Maximum incremental facing displacements for earthquake motions (model-scale).

Earthquake motion	T1-South		T1-North		L1	
	Dynamic displacement (mm)	Residual displacement (mm)	Dynamic displacement (mm)	Residual displacement (mm)	Dynamic displacement (mm)	Residual displacement (mm)
Imperial Valley	5.1	1.1	5.2	1.1	1.6	1.2
Maule	17.0	2.2	9.3	1.7	3.2	2.6
Northridge	34.7	9.4	13.3	0.5	4.0	3.2

Table 4. Average incremental bridge seat settlements for earthquake motions (model-scale).

Earthquake motion	Maximum dynamic settlement (mm)	Minimum dynamic settlement (mm)	Residual settlement (mm)
Imperial Valley	3.3	0.0	2.5
Maule	9.5	-0.1	4.8
Northridge	6.1	-2.1	4.7

Table 5. Average incremental residual bridge seat settlements for longitudinal and transverse shaking (model-scale).

Earthquake motion	Longitudinal shaking settlement (mm)	Transverse shaking settlement (mm)
Imperial Valley	1.4	2.5
Maule	1.4	4.8
Northridge	2.2	4.7

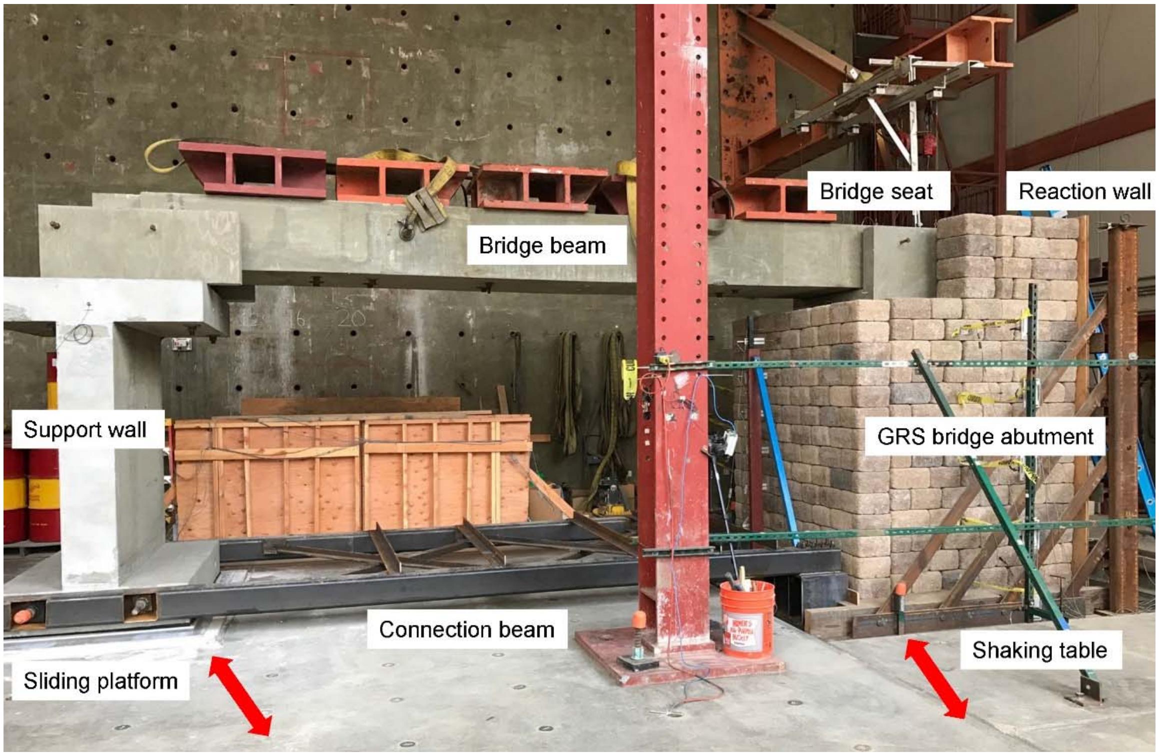

Figure 1. Configuration of GRS bridge abutment system (shaking direction indicated by red arrows).

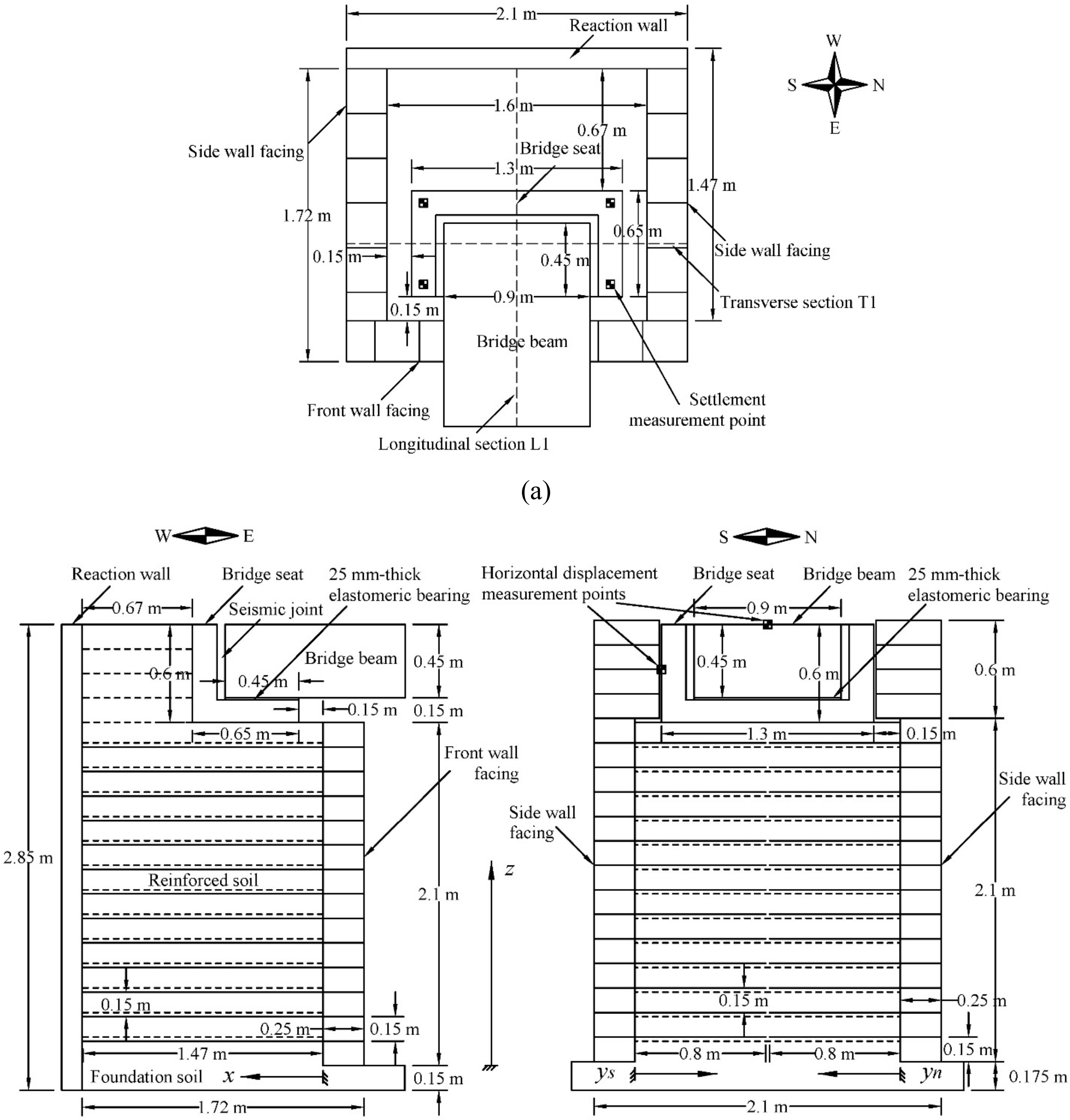

(b) (c)

Figure 2. GRS bridge abutment model: (a) top view; (b) longitudinal cross-sectional view; (c) transverse cross-sectional view. Note: dashed lines indicate reinforcement layers perpendicular to diagram.

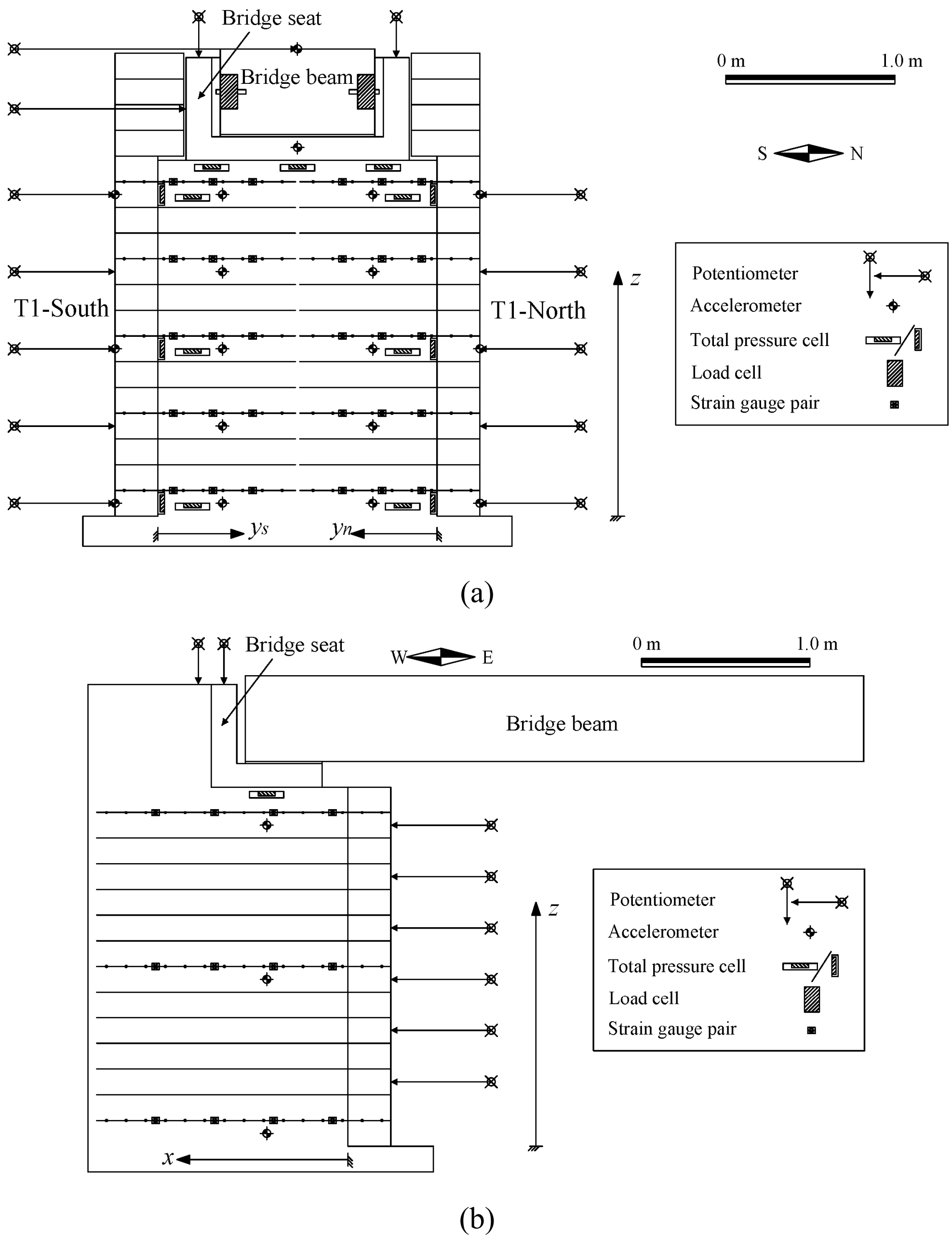

Figure 3. Instrumentation: (a) transverse section T1 (x = 0.48 m); (b) longitudinal section L1 (y_n = 0.8 m).

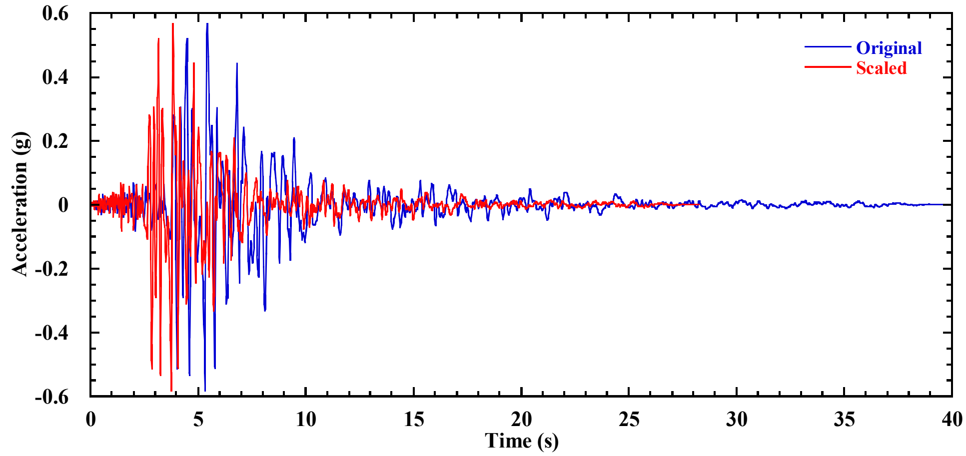

(a)

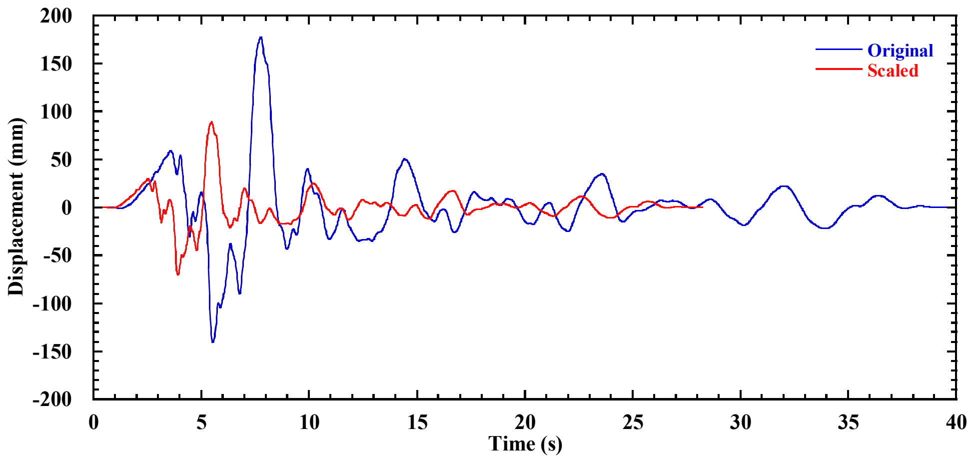

(b)

Figure 4. Original records and scaled motions for the 1994 Northridge earthquake (Newhall station): (a) acceleration time history; (b) displacement time history.

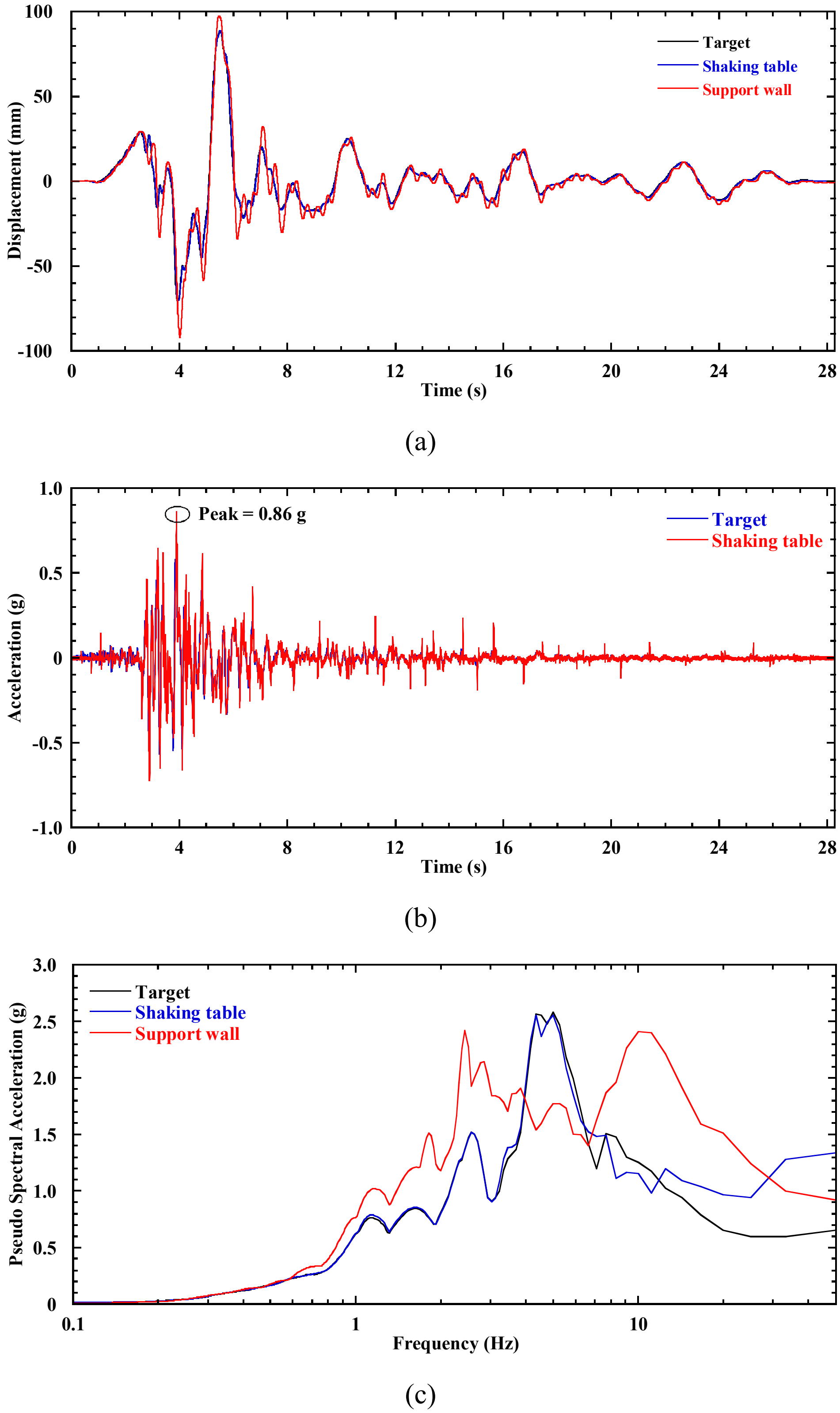

Figure 5. Testing system response for the Northridge motion: (a) displacement time history; (b) acceleration time history; (c) response spectra (5% damping).

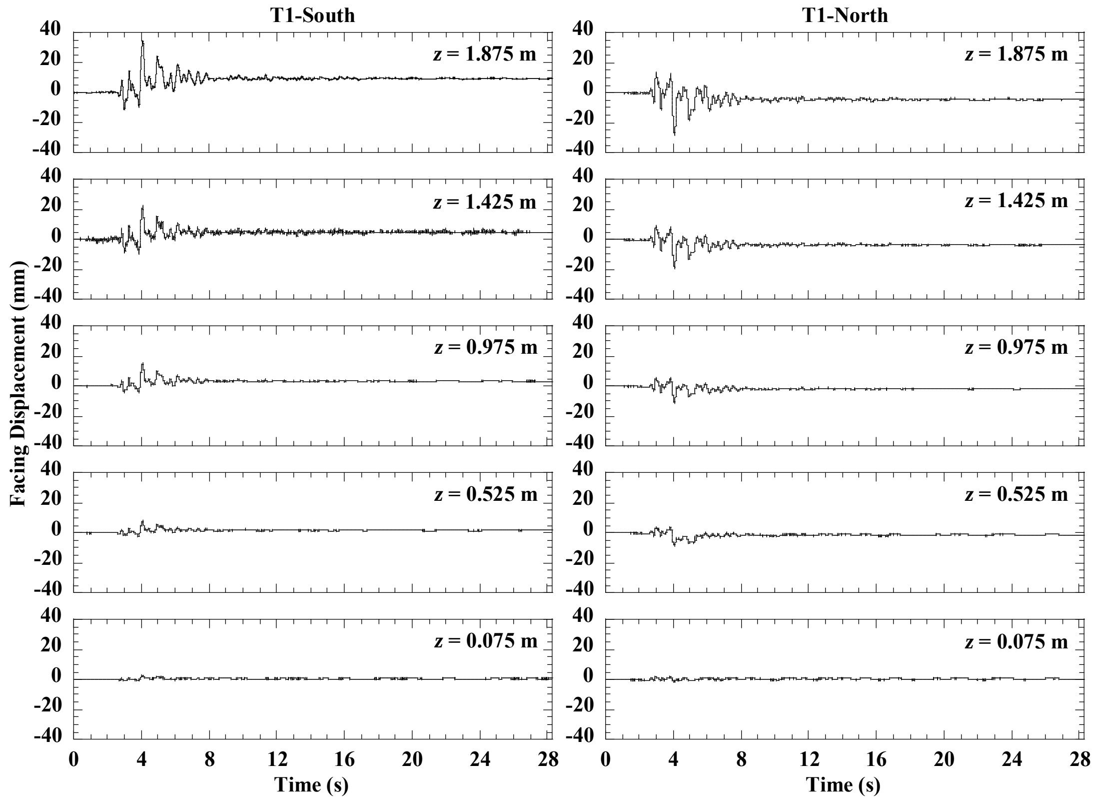

Figure 6. Time histories of incremental facing displacement for walls T1-South and T1-North during the Northridge motion.

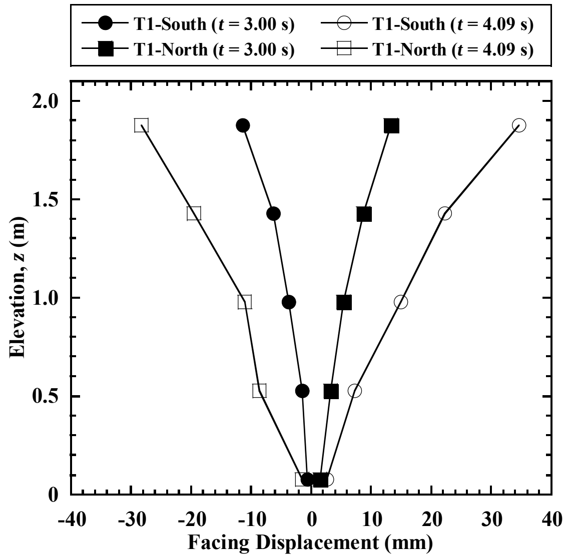

Figure 7. Incremental dynamic facing displacement profiles for walls T1-South and T1-North during the Northridge motion.

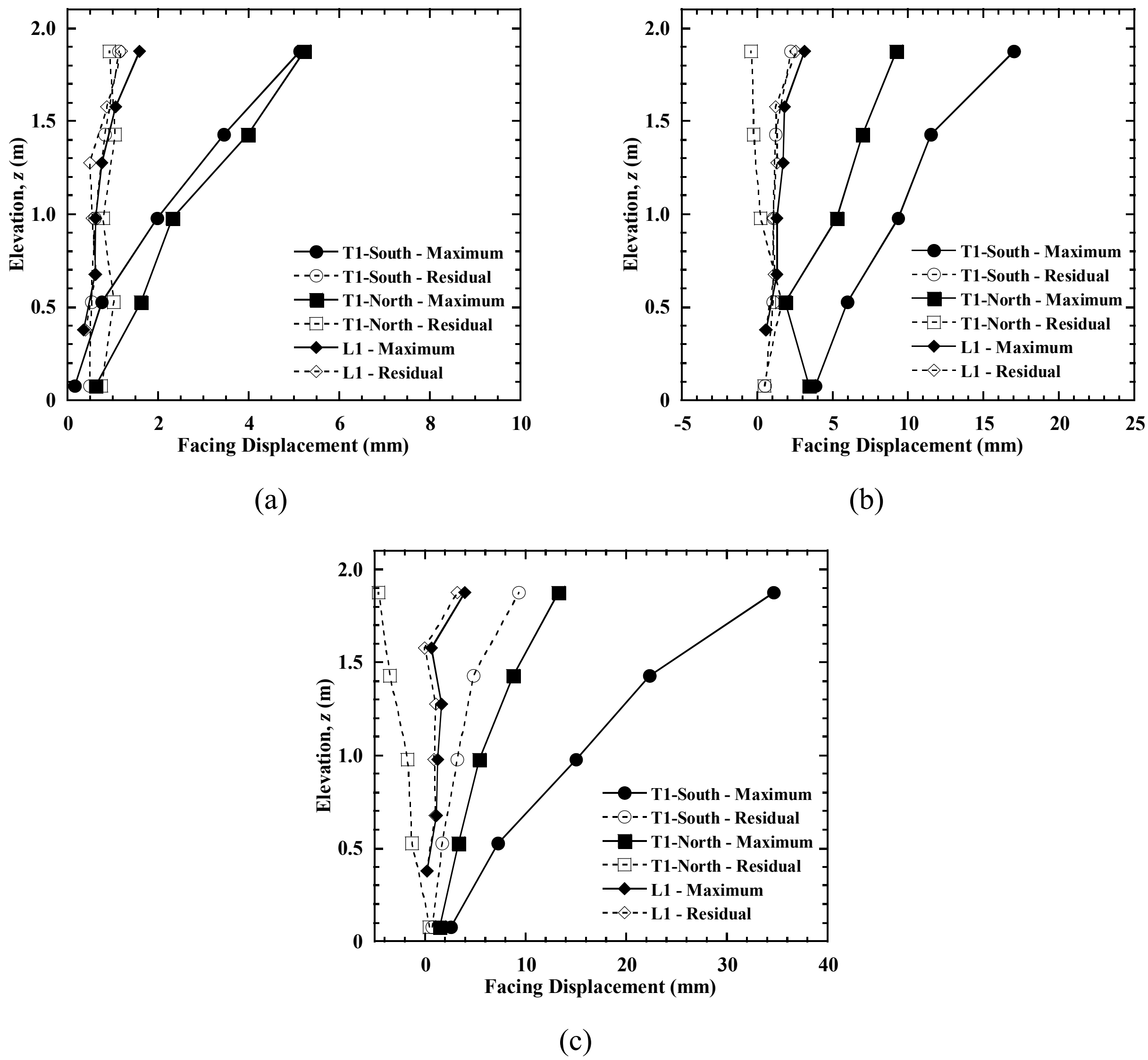

Figure 8. Incremental facing displacement profiles: (a) Imperial Valley motion; (b) Maule motion; (c) Northridge motion.

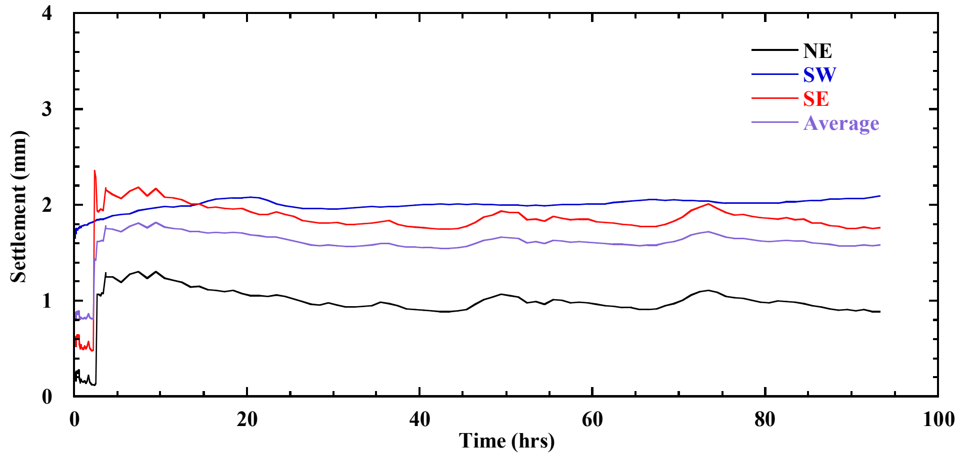

(a)

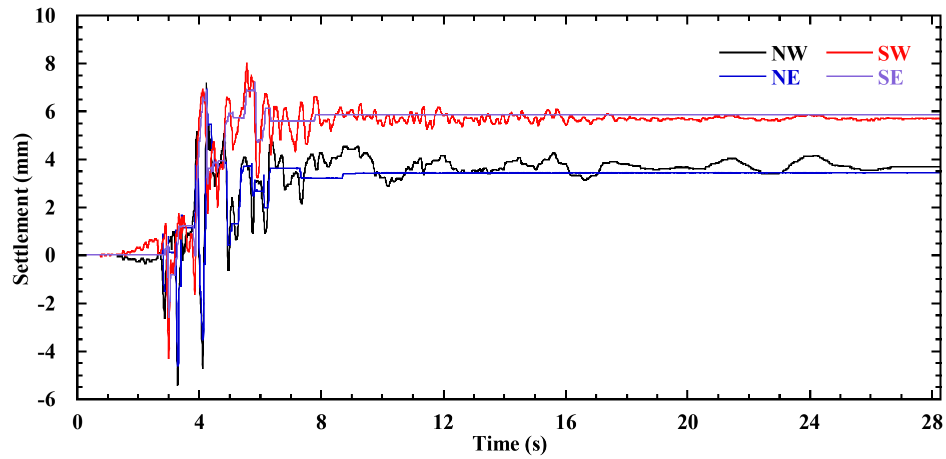

(b)

Figure 9. Time histories of incremental bridge seat settlements: (a) during placement of the bridge beam; (b) during the Northridge motion.

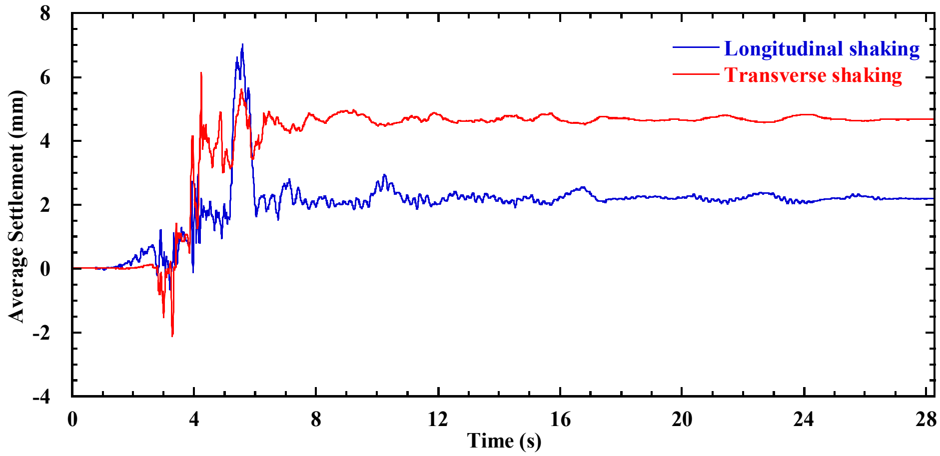

Figure 10. Time histories of average incremental bridge seat settlements for longitudinal and transverse shaking during the Northridge motion.

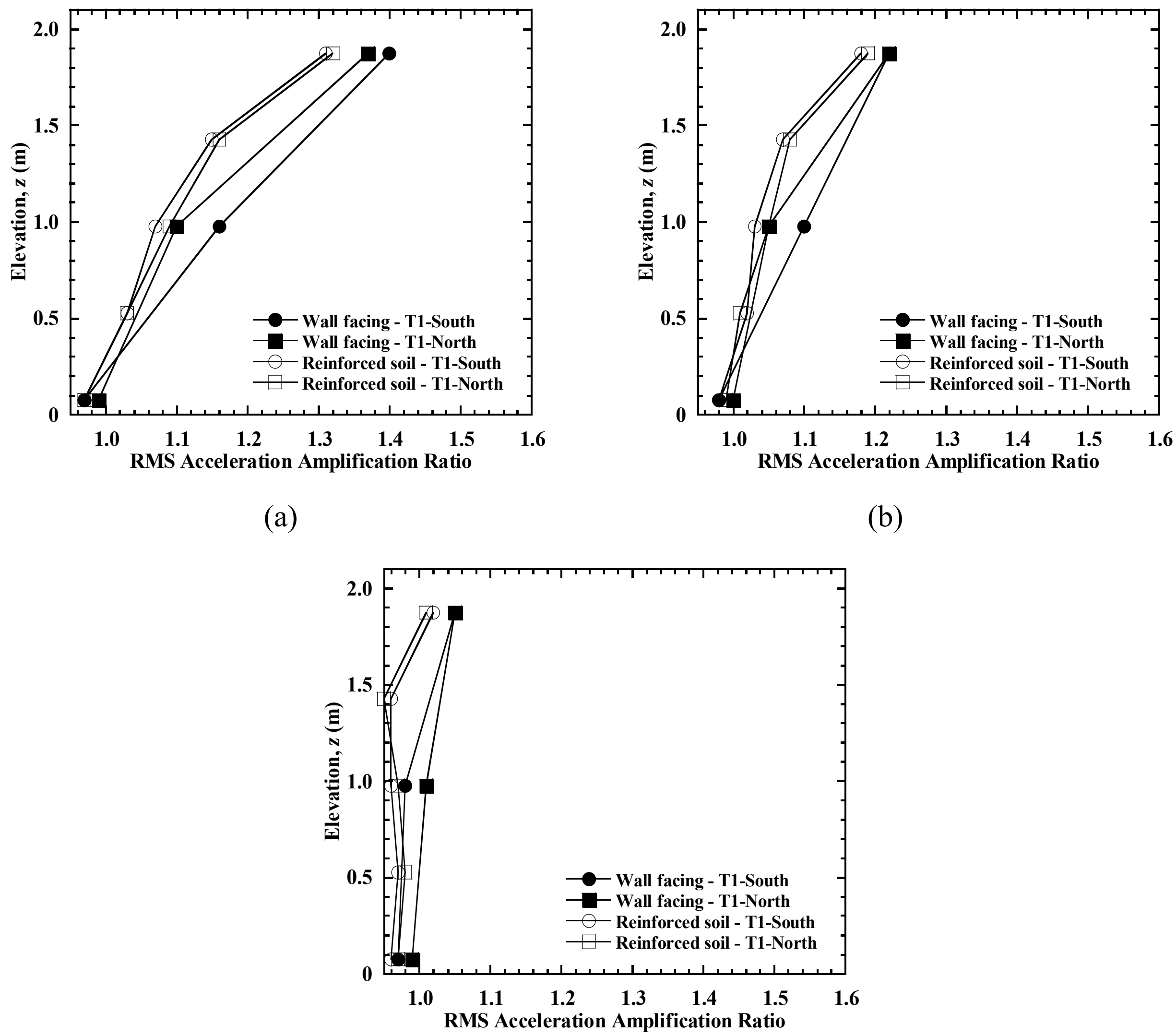

(a) (b)

(c)

Figure 11. RMS acceleration amplification ratio profiles for the T1-South and T1-North walls: (a) Imperial Valley motion; (b) Maule motion; (c) Northridge motion.

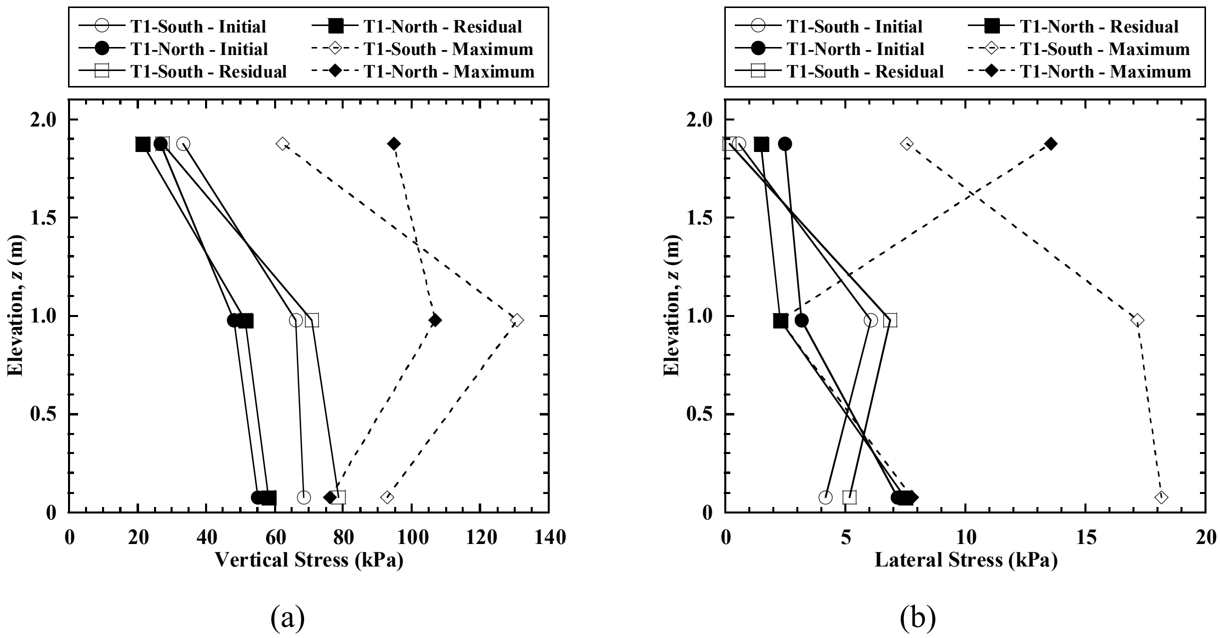

Figure 12. Soil stress profiles for the T1-South and T1-North walls during the Northridge motion: (a) vertical stress; (b) lateral stress.

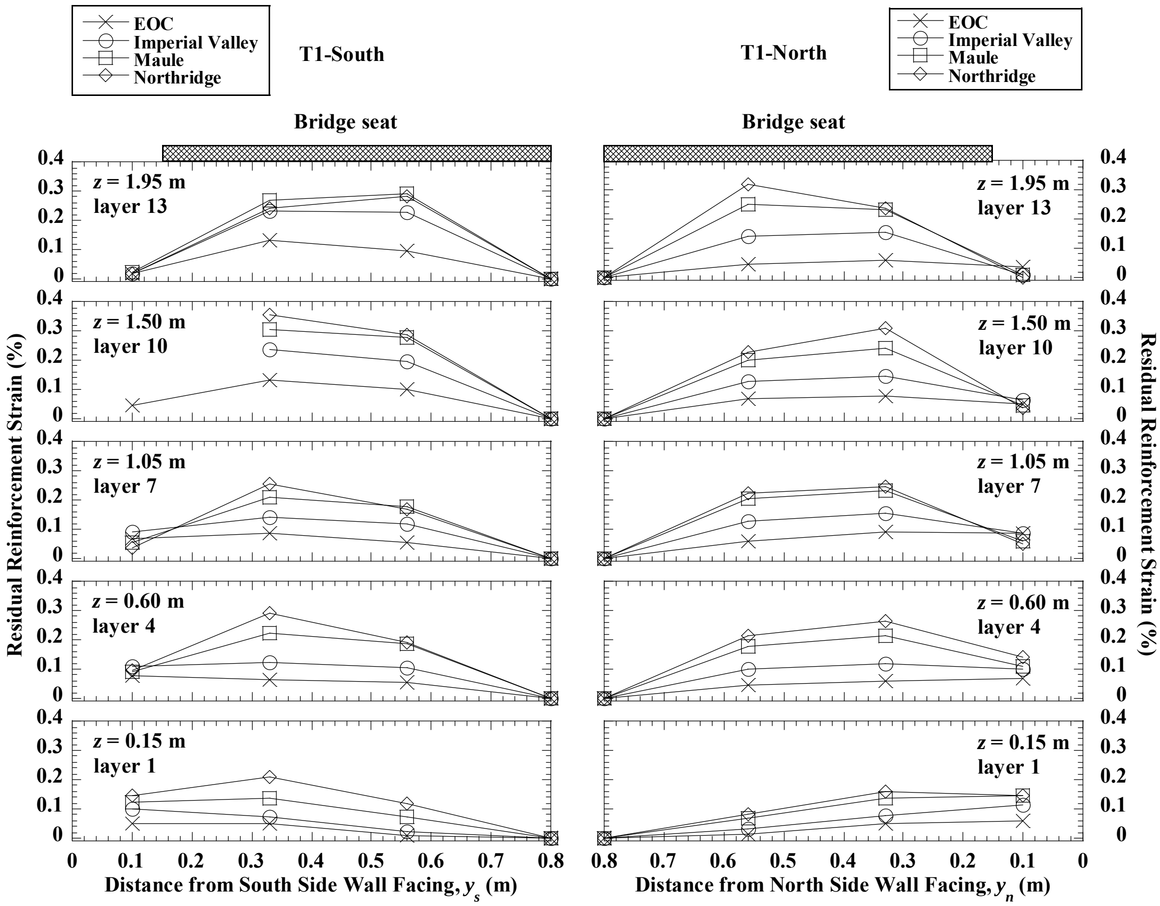

Figure 13. Residual reinforcement strain distributions for the T1-South and T1-North walls.

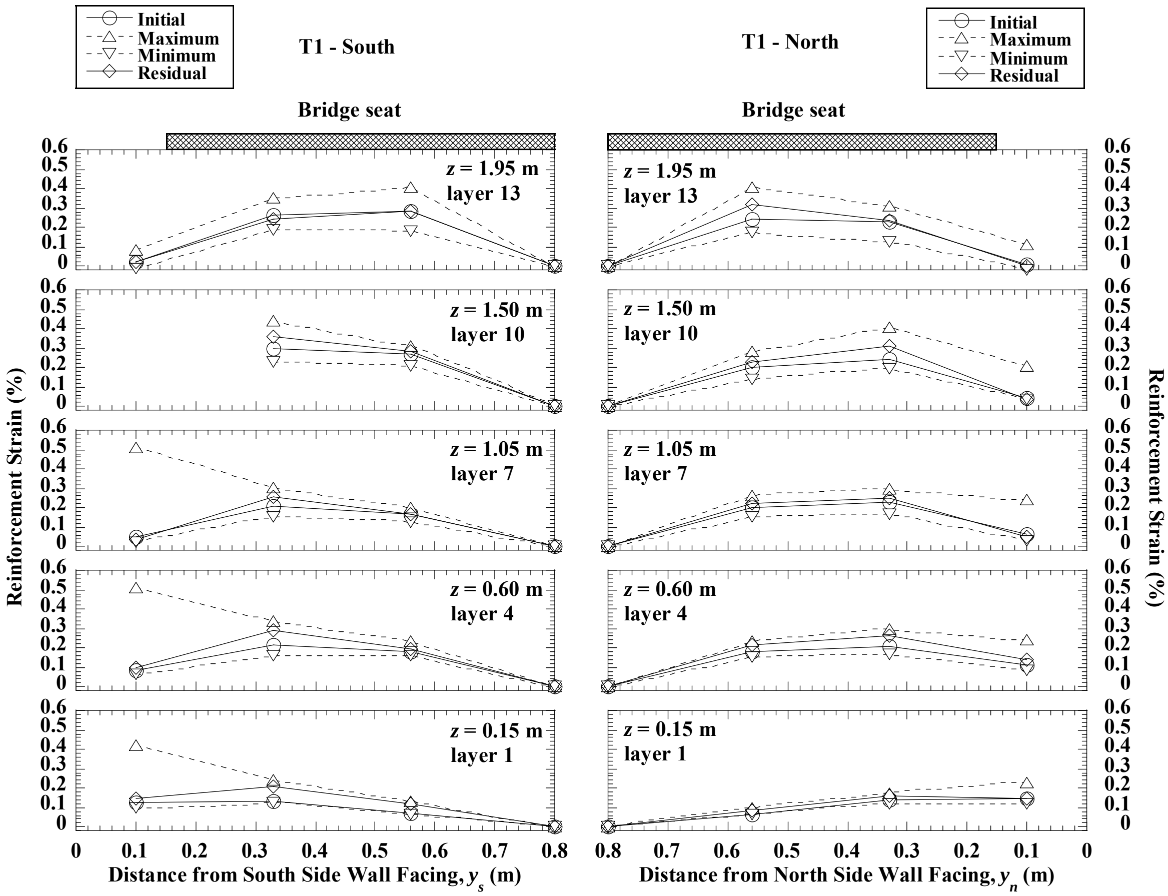

Figure 14. Reinforcement strain distributions for the T1-South and T1-North walls during the Northridge motion.

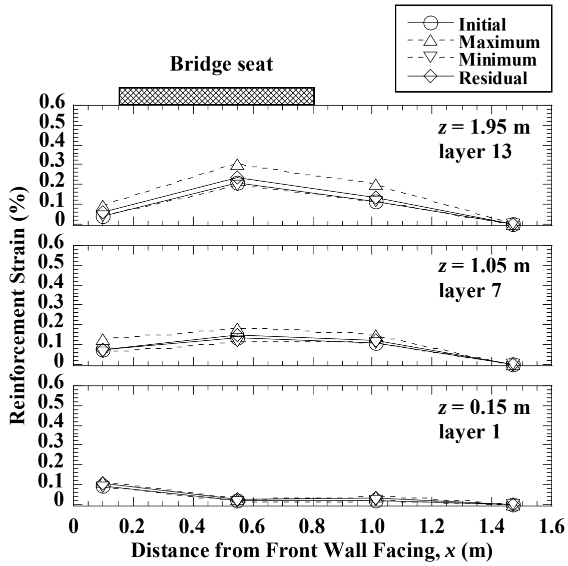

Figure 15. Reinforcement strain distributions for the L1 wall during the Northridge motion.

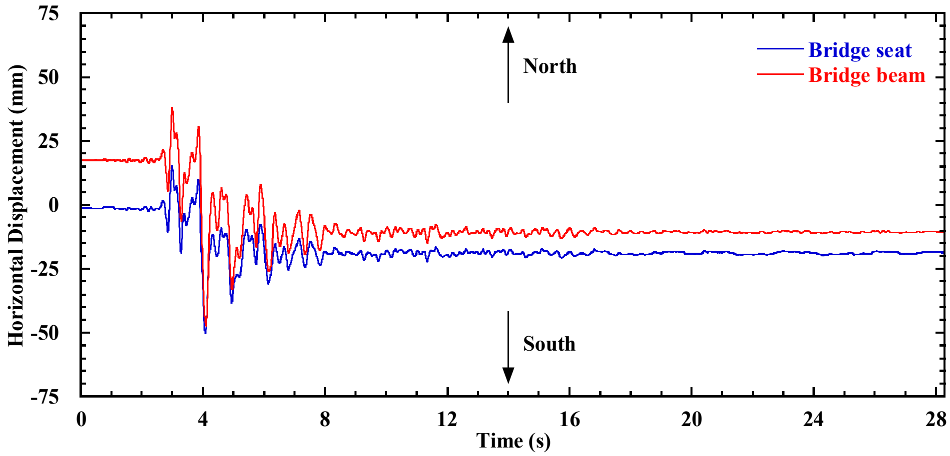

(a)

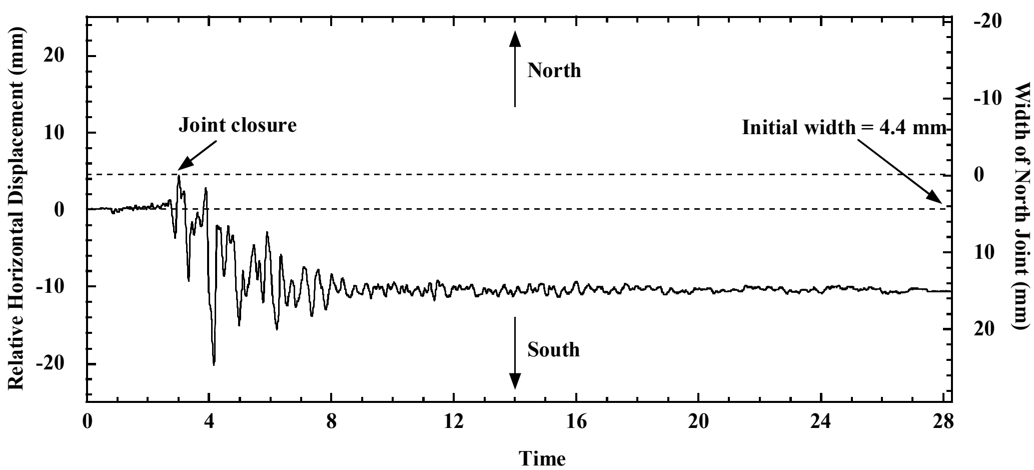

(b)

Figure 16. Time histories of horizontal displacements for bridge seat and bridge beam during the Northridge motion: (a) incremental horizontal displacements; (b) incremental relative horizontal displacements of bridge beam relative to bridge seat.

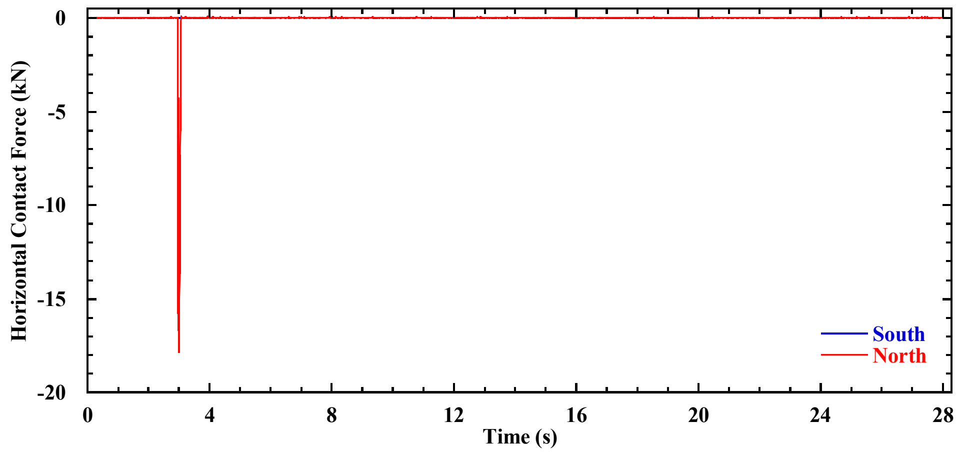

Figure 17. Time histories of horizontal contact forces between the bridge seat and bridge beam during the Northridge motion.